Crystal-field effects in the mixed-valence compounds $Yb_2M_3Ga_9$ (M=Rh,Ir)

N. O. Moreno,[1] A. Lobos,[2] A. A. Aligia,[2] E. D. Bauer,[1] S. Bobev,[1,*] V. Fritsch,[1] J. L. Sarrao,[1] P. G. Pagliuso,[1] J. D. Thompson,[1] C. D. Batista,[1] and Z. Fisk[3,†]

[1]*Los Alamos National Laboratory, Los Alamos, New Mexico 87545, USA*

[2]*Centro Atómico Bariloche and Instituto Balseiro, Comisión Nacional de Energía Atómica, 8400 S.C. de Bariloche, Argentina*

[3]*Department of Physics, University of California, Davis, California 95616, USA*

(Received 4 October 2004; revised manuscript received 31 January 2005; published 12 April 2005)

Magnetic susceptibility, heat capacity, and electrical resistivity measurements have been carried out on single crystals of the intermediate valence compounds $Yb_2Rh_3Ga_9$ and $Yb_2Ir_3Ga_9$. These measurements reveal a large anisotropy due apparently to an interplay between crystalline electric field (CEF) and Kondo effects. The temperature dependence of magnetic susceptibility can be modelled using the Anderson impurity model including CEF within an approach based on the non-crossing approximation.

DOI: 10.1103/PhysRevB.71.165107 PACS number(s): 71.27.+a, 71.28.+d, 75.30.Mb, 75.20.Hr

I. INTRODUCTION

The intermediate valence compounds pose one of the most challenging problems of strongly correlated electron systems. Different ingredients contribute to the complexity of these fascinating systems: the presence of strong Kondo interactions, the level structure of the crystal electric field (CEF) f orbitals, the different hybridizations between each level and the conduction band, and the eventual coherence effects and magnetic interactions introduced by the periodicity of the Kondo lattice.[1] Strong valence fluctuations are observed in the intermetallic compounds with Ce, Yb, and U. In particular, Yb compounds attract a great deal of interest because the trivalent Yb ion is at least in some sense the hole counterpart of the Ce^{3+} ion which has one electron in its $4f$ shell. As in the case of the Ce compounds,[2] the Yb-based intermetallics exhibit a diversity of physical properties that remain to be understood.[3]

The isostructural series of compounds $R_2M_3X_9$ (R=La, Ce, Yb, U; M=Co, Rh, Ir; X=Al, Ga) exhibit antiferromagnetic ordering for R=Yb, X=Al, and mixed-valence behavior for R=Ce,Yb and X=Ga.[4–7] All the U-based compounds order antiferromagnetically at temperatures below 40 K.[4] The $Yb_2M_3Ga_9$ compounds are a suitable class of materials for studying the difference in the electronic structure between the magnetically ordered Kondo lattice and the mixed-valence systems. The orientation-dependent temperature T_{max} of the maximum in the magnetic susceptibility suggests the possibility of an anisotropic Kondo effect.[8,9] Previously, Petrovic *et al.* studied ternary R-Ir—Ga compounds (R =rare earth) that were assigned the RIr_2Ga stoichiometry in their work.[10–12] Elemental analysis studies unavailable to these previous authors suggest that $R_2Ir_3Ga_9$ is the correct stoichiometry of these materials instead. The $R_2Ir_3Ga_9$ compounds with Ce and Yb show reduced magnetic moments and the absence of magnetic order above 0.04 K.[11]

The thermodynamic properties of the single-impurity model have been calculated exactly using the Bethe-ansatz technique,[14–18] and also approximately within the non-crossing approximation (NCA), which shows good agreement with the former.[19] However, to the best of our knowledge, it has always been assumed that the hybridization V_m between any state of the magnetic configuration $|m\rangle$ and the conduction electrons is independent of m even when the CEF is included.[14–16] This is a requirement for the integrability of the problem;[20] although, there is no symmetry requirement to have the same V_m for each orbital in the presence of a CEF. The different orientations of the orbitals relative to the nearest-neighbor atoms clearly indicate that the hybridizations must be a function of m. It is essential to consider this effect in order to explain the magnetic susceptibility $\chi(T)$ measurements of $Yb_2M_3Ga_9$ (M=Rh,Ir) shown here as well as various other experimental observations in related materials.[21]

Here, we report two examples of mixed-valence systems, $Yb_2Rh_3Ga_3$ and $Yb_2Ir_3Ga_9$, in which the CEF and Kondo energy scales are of the same order of magnitude. We discuss a method based on the simple approximation scheme of Zwicknagl *et al.* for calculating dynamical and static properties for these types of systems.[22] The novelty of the method is that, in addition to the usual CEF effects, it also incorporates the important consequences of having different hybridization amplitudes $V(m)$ between the CEF orbitals and the conduction band. The calculated $\chi(T)$ provides a quantitative description of the measured susceptibility in $Yb_2M_3Ga_9$ (M =Rh,Ir). We show that for $Yb_2Ir_3Ga_9$ a single hybridization $V(m)$ is sufficient to describe the data, whereas for $Yb_2Rh_3Ga_9$, two hybridizations are necessary to adequately describe our results.

II. EXPERIMENT

Single crystalline rods of $Yb_2M_3Ga_9$ (M=Rh,Ir) with a tapered hexagonal morphology were grown by a Ga self-flux technique. Elemental analysis confirmed the correct 2-3-9 stoichiometry. X-ray powder diffraction measurements on crushed single crystals produce a spectrum that can be indexed in either a hexagonal or C-centered orthorhombic structure. Examination of the resulting lattice parameters suggests that the hexagonal unit cell is apparently a subcell of a larger orthorhombic cell (with $a_{orthorhombic}=\sqrt{3}a_{hexagonal}$). The room-temperature values of the hexagonal lattice parameters are a=7.471(6) Å, c=9.440(3) Å for $Yb_2Rh_3Ga_9$ and a=7.483(4) Å, c=9.441(2) Å for $Yb_2Ir_3Ga_9$, in agreement with Refs. 6 and 11. The larger orthorhombic lattice con-

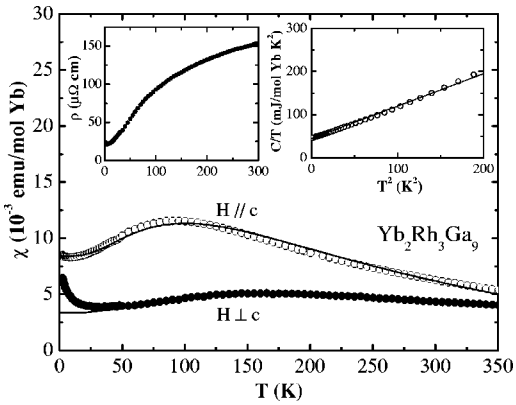

FIG. 1. Magnetic susceptibility $\chi(T)$ of $Yb_2Rh_3Ga_9$. The lines are fits to the data using the model described in the text. Left-hand inset, electrical resistivity $\rho(T)$ of $Yb_2Rh_3Ga_9$. Right-hand inset, specific heat divided by temperature C/T versus T^2 of $Yb_2Rh_3Ga_9$.

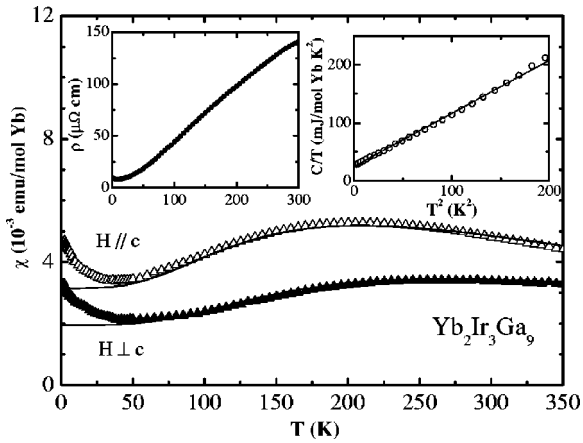

FIG. 2. Magnetic susceptibility $\chi(T)$ of $Yb_2Ir_3Ga_9$. The lines are fits to the data using the model described in the text. Left-hand inset, electrical resistivity $\rho(T)$ of $Yb_2Ir_3Ga_9$. Right-hand inset, specific heat divided by temperature C/T versus T^2 of $Yb_2Ir_3Ga_9$.

stants are close to those reported for polycrystalline samples of the same compounds obtained by means of arc or induction melting.[4,23,24] X-ray single crystal diffraction studies (discussed in detail elsewhere[12]) that include the possible role of stacking fault disorder, as indicated in isostructural aluminum-rich compounds,[13] suggest that the samples crystallize in the hexagonal structure. Specific heat and magnetization measurements were performed in a commercial (Quantum Design) PPMS and MPMS, respectively. The resistivity was measured using a standard four-probe technique, with the current parallel to the c axis in the temperature range of 0.5–300 K under zero applied field.

Figure 1 shows the magnetic susceptibility, $\chi(T)$, of $Yb_2Rh_3Ga_9$ measured in $H=1$ kOe. $\chi(T)$ displays a broad maximum at 90 K ($H\|c$) and 165 K ($H\perp c$), typical of mixed-valence compounds. The high-temperature magnetic susceptibility of $Yb_2Rh_3Ga_9$ follows a Curie-Weiss law above 200 K yielding values of $\mu_{\rm eff}=4.3\ \mu_B/\text{Yb}$; $\theta=-50$ K and $\mu_{\rm eff}=4.4\ \mu_B/\text{Yb}$; $\theta=-293$ K for field parallel and perpendicular to the c axis, respectively. The average effective magnetic moment is nearly the value of free Yb^{3+} ($\mu_{\rm eff}=4.5\ \mu_B$). The marked difference in the respective values for the Weiss temperature is due to the strong magnetocrystalline anisotropy. As will be discussed later, this anisotropy is also the origin of the orientation-dependent maxima in $\chi(T)$.

Figure 2 displays magnetic susceptibility data for $Yb_2Ir_3Ga_9$. These data are consistent with stronger hybridization in $Yb_2Ir_3Ga_9$ as compared with $Yb_2Rh_3Ga_9$. The maxima in $\chi(T)$ are shifted to higher temperature, and Curie-Weiss behavior is not fully recovered by our highest measurement temperature. As pointed out by Trovarelli *et al.*,[6] the upturns in susceptibility at lowest temperature may not be extrinsic. These authors reach this conclusion based on field-dependent magnetization measurements. That we see field-orientation dependent upturns at low temperature, especially in the case of $Yb_2Rh_3Ga_9$ [$\chi(T)$ for $H\|c$ is essentially temperature independent whereas $\chi(T)$ for $H\perp c$ increases rapidly with decreasing temperature] adds further credibility to this assertion.[6]

The electrical resistivity $\rho(T)$, measured with current applied along the hexagonal c-axis (the long axis of our rodlike crystals), of $Yb_2Rh_3Ga_9$ and $Yb_2Ir_3Ga_9$ is displayed on the left-hand insets of Figs. 1 and 2, respectively. The observed temperature dependences are characteristic of intermediate-valence metals and again reflect the higher characteristic temperature (i.e., the inflection point) in $Yb_2Ir_3Ga_9$. Similarly, specific heat divided by temperature C/T versus T^2 is shown on the right-hand insets of Figs. 1 and 2 for $M=$Rh, Ir, respectively. A low-temperature fit to $C/T=\gamma+\beta T^2$ gives values of $\gamma=45(25)$ mJ/mol Yb K^2 and $\beta=0.75(0.91)$ mJ/mol Yb K^4, corresponding to a Debye temperature $\theta_D=250$ K (234 K) for $M=$Rh (Ir). The values of γ reflect moderate mass enhancement in $Yb_2Rh_3Ga_9$ and $Yb_2Ir_3Ga_9$.

III. THEORY

To account for the combined effects of Kondo hybridization and crystal electric field splitting, we use an approximation scheme developed in Refs. 22 and 25 that we generalize to allow for different conduction electron hybridizations of each ground state multiplet of the magnetic configuration. The approach is based on the non-crossing approximation (NCA) with the additional assumption that the density of states of the nonmagnetic configuration by its pole at temperature $T=0$,

$$\rho_0(\omega) = (1 - n_f)\,\delta(\omega - \omega_0), \tag{1}$$

where $2+n_f$ is the valence of Yb at $T=0$, and ω_0 is the ground state energy, obtained by a variational ansatz that is exact for large degeneracy of the magnetic configuration.[26] The approximation Eq. (1) ceases to be valid at temperatures of the order of the charge transfer energy $E_0-\min(E_m)+\epsilon_F$ (see below). However, it has led to very good agreement with results for the magnetic susceptibility of the full NCA and Bethe-ansatz in the isotropic case.[22] Furthermore, it has the advantage that the results converge smoothly to those of the variational approximation for $T=0$ and is free from the usual artifacts of the NCA at low T.[27,28]

The Hamiltonian is that of the impurity Anderson model including crystal and magnetic field,

$$H = H_0 + H_1 + H_B + H_{\text{band}} + H_{\text{mix}}, \tag{2}$$

with

$$H_0 = E_0|0\rangle\langle 0|, \quad H_1 = \sum_m E_m|m\rangle\langle m|,$$

$$H_B = -g\mu_B B J_\alpha, \quad H_{\text{band}} = \sum_{km} \epsilon_k c_{km}^\dagger c_{km}, \tag{3}$$

$$H_{\text{mix}} = \sum_{km} V_m(|m\rangle\langle 0|c_{km} + \text{H.c.}).$$

H_0 describes the ground state of the nonmagnetic $4f^{14}$ configuration of Yb^{+2}; H_1 corresponds to the ground state multiplet of the $4f^{13}$ configuration, distributed in four Kramers degenerate doublets belonging to three irreducible representations of the point group; $c_{km}^\dagger$ creates a hole in an extended state with the same symmetry as the localized state $|m\rangle$. The density of these band states ρ is assumed constant and independent of m as usual. The term H_{mix} allows for different hybridizations V_m for each doublet. H_B describes the coupling of the magnetic configuration with an applied magnetic field B in the direction α. The value of g for Yb is $8/7$.

To be able to use the NCA at finite B when V_m depends on m, we diagonalize first H_1+H_B and perform a canonical transformation on the $c_{km}^\dagger$ in such a way that H_1+H_B takes the form of H_1 with field dependent E_m, and H_{mix} retains the same form in the new basis. Calling $|m(B)\rangle$ the eigenstates of H_1+H_B, the transformation is

$$c_{km}^\dagger(B) = \frac{1}{V_m(B)} \sum_{m'} V_{m'} \langle m'(0)||m(B)\rangle c_{km'}^\dagger, \tag{4}$$

where

$$V_m^2(B) = \sum_{m'} V_{m'}^2 |\langle m'(0)||m(B)\rangle|^2. \tag{5}$$

Working up to second order in B, diagonalizing first J_α in each subspace of identical E_m, denoting $\Gamma_m = \pi\rho V_m^2$, we obtain for $E_m(B)$ and $\Gamma_m(B)$ in the new basis,

$$E_m = E_m^0 - g\mu_B B\langle m|J_\alpha|m\rangle + (g\mu_B B)^2 \sum_{m'}' \frac{|\langle m|J_\alpha|m'\rangle|^2}{E_m^0 - E_{m'}^0},$$

$$\Gamma_m = \Gamma_m^0 + (g\mu_B B)^2 \sum_{m'}' \frac{(\Gamma_{m'}^0 - \Gamma_m^0)|\langle m|J_\alpha|m'\rangle|^2}{(E_m^0 - E_{m'}^0)^2}, \tag{6}$$

where $\Sigma_{m'}'$ runs over all m' with $E_{m'}^0 \neq E_m^0$ and $E_m^0 = E_m(0)$, $\Gamma_m^0 = \Gamma_m(0)$. In this way the Hamiltonian is mapped into $H - H_B$ with field dependent parameters.

Proceeding as in Ref. 26, the ground state energy $\omega_0(B)$ is obtained from the equation

$$\omega_0 - E_0 = \sum_m \frac{\Gamma_m}{\pi} \ln \frac{E_m - \omega_0}{W + E_m - \omega_0}, \tag{7}$$

where we set the Fermi energy ϵ_F to zero and W is the width of the part of the conduction band occupied with holes. Using $\chi_\alpha(0) = -\partial^2\omega_0/\partial B^2$ and neglecting $1/W$ in comparison with $1/T_0$, where $T_0 = \min(E_m) - \omega_0$ is the stabilization energy of the correlated singlet, we obtain a closed expression for the susceptibility at $T=0$,

$$\chi_\alpha(0) = (g\mu_B)^2 \sum_m n_{fm} \left[\frac{\langle m|J_\alpha|m\rangle}{E_m^0 - \omega_0} + 2\sum_{m'}' |\langle m|J_\alpha|m'\rangle|^2 \times \left(\frac{1}{E_{m'}^0 - E_m^0} + \frac{E_m^0 - \omega_0}{(E_m^0 - E_{m'}^0)^2} \ln \frac{E_m^0 - \omega_0}{E_{m'}^0 - \omega_0} \right) \right], \tag{8}$$

where n_{fm}, the occupation number of the state $|m\rangle$ at $T=0$, is given by

$$n_{fm} = \frac{C_m}{1 + \sum_n C_n}, \quad C_m = \frac{\Gamma_m}{\pi(E_m - \omega_0)}. \tag{9}$$

The same expression Eq. (8) is obtained finding first the variational wave function for $B=0$ and then using second order perturbation theory in B. While this procedure is actually easier, it cannot be extended to $T \neq 0$.

At finite T, the susceptibility is obtained from $\chi_\alpha(T) = -\partial^2 F/\partial B^2$, where the free energy is given by

$$F = \omega_0 - T \ln\left[(1 - n_f)\left(1 + \sum_m \Gamma_m I_m\right)\right], \tag{10}$$

with:

$$n_f = \sum_m n_{fm}, \tag{11}$$

$$I_m = \int \frac{d\omega}{\pi} \frac{f(\omega)}{(\omega + \omega_0 - E_m)^2 + [\Gamma_m(1 - n_f)f(-\omega)]^2}, \tag{12}$$

where $f(\omega)$ is the Fermi function. The second derivative of F is calculated using Eqs. (6), (9), and (11).

Up to now the theory corresponds to a single magnetic impurity coupled to band states. We find that in order to explain the observed magnetic susceptibility, in particular the ratio of $\chi(T=0)$ and the maximum value of $\chi(T)$, a small antiferromagnetic interaction between Yb ions should be included. In mean field, the susceptibility of the compound χ_α^c is given by

$$\chi_\alpha^c = \frac{\chi_\alpha}{1 + I\chi_\alpha}, \quad I = \frac{\sum_\delta J_\delta}{(g\mu_B)^2}, \tag{13}$$

where the sum runs over the exchange interactions of all sites that interact with the given one.

IV. DISCUSSION

The best fits to the anisotropic magnetic susceptibility data for $Yb_2Rh_3Ga_9$ and $Yb_2Ir_2Ga_2$ using our theoretical framework are shown in Figs. 1 and 2, respectively. The parameters associated with these fits are given in Table I. To obtain these fits in practice, we use n_f at $T=B=0$ rather than

TABLE I. Fit parameters for the three calculations of the magnetic susceptibility of $Yb_2M_3Ga_9$ (M=Rh,Ir) described in the text. T_K Kondo temperature. The values of the energy scale T_0 for the NCA calculations have been scaled to compare with the Bethe-ansatz Kondo temperature T_K. The scale factor is given by $T_K=[(2J+1)/2\pi n_f]T_0$, yielding the values of T_K listed in the table. I, molecular field constant; Γ, (single) conduction electron hybridization with CEF states; Γ_m^0, conduction electron hybridization with CEF state $|m\rangle$; Δ, CEF splitting between upper and lower quartets; n_f, f-occupation number at $T=0$ K; γ, electronic specific heat coefficient; GOF for $\chi\parallel/\perp c$, $(1/N)\Sigma_{i=1}^N[(\chi_i^{\rm exp}-\chi_i^{\rm th})/\sigma_i^{\rm exp}]^2/d$, where N is the number of data points, $\sigma_i^{\rm exp}$ is the error in $\chi_i^{\rm exp}$, and d is the number of degrees of freedom (Ref. 29). The units of T_K, Δ, and Γ are K; units of I are mol Yb/emu; units of γ are mJ/mol Yb K^2.

	Bethe-ansatz			NCA, single CEF hybridization						NCA, multiple CEF hybrizations							
Compound	T_K	I	Γ	Δ	I	T_K	n_f	γ	GOF	$\Gamma^0_{\pm7/2,\pm5/2}$	$\Gamma^0_{\pm3/2,\pm1/2}$	Δ	I	T_K	n_f	γ	GOF
$Yb_2Rh_3Ga_9$	550	10	165	400	25	419	0.59	68	2.51/9.10	170	145	400	25	429	0.59	68	2.51/0.59
$Yb_2Ir_3Ga_9$	1000	20	230	280	45	1030	0.53	28									

E_0 and W as fitting parameters and determine ω_0 from Eqs. (9) and (11). Because the upturns in susceptibility at low temperature are either extrinsic or periodic effects beyond the scope of our model, only data above 50 K were used in our fits. Several considerations influenced our fitting of the data in order to minimize the number of allowed free parameters. In order to obtain a larger susceptibility for B parallel to the c axis ($\chi_\parallel$), states with larger angular momentum projection along that axis m_c should lie lower in energy. However, the well-defined maximum in $\chi_\parallel$ at intermediate temperatures ($T_{\max}\sim 100$ K) points to an effective large degeneracy (this is clear from Bethe-ansatz results in the isotropic case.[17]) As a compromise, we took a fourfold degenerate ground state of H_1, containing the states with $m_c=\pm7/2$ and $m_c=\pm5/2$ along c (all belonging to the same irreducible representation). The remaining four states were also assumed degenerate. Allowing these quartets to split into closely spaced doublets does not qualitatively change the results. A larger admixture with the $4f^{14}$ configuration (lower n_f) decreases both susceptibilities but increases relatively the upturn in $\chi_\parallel$ as pointed out earlier.[22]

The structure of the compounds suggest a larger hybridization for orbitals lying in the plane perpendicular to the c axis, which should correspond to higher m_c. Thus, we begin our fitting procedure with two different values of Γ_m, with the larger value corresponding to the ground state quartet. Increasing Γ_m for both quartets leads to flatter curves and more similar values of $\chi_\parallel$ and $\chi_\perp$. As indicated in Table I, a single hybridization parameter (i.e., $\Gamma\equiv\Gamma^0_{\pm7/2}=\Gamma^0_{\pm5/2}=\Gamma^0_{\pm3/2}=\Gamma^0_{\pm1/2}$) is sufficient to produce a high quality fit to the data for $Yb_2Ir_3Ga_9$ (Fig. 2). It is worth noting, however, that the included crystal field splitting is essential for describing the data.

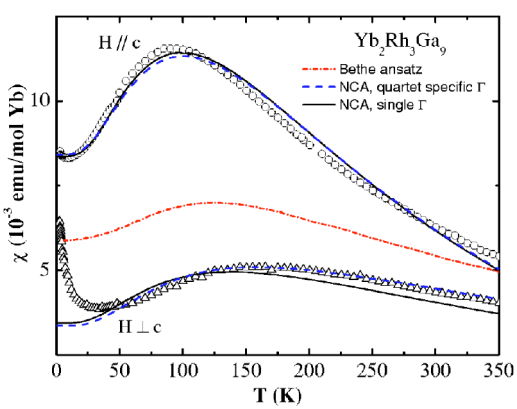

FIG. 3. (Color online) Magnetic susceptibility $\chi(T)$ of $Yb_2Rh_3Ga_9$. The lines are fits to the data of the three calculation approaches discussed in the text.

As the overall hybridization decreases from $Yb_2Ir_3Ga_9$ to $Yb_2Rh_3Ga_9$, the need for level-specific hybridization becomes apparent. In order to adequately fit the susceptibility of $Yb_2Rh_3Ga_9$, especially the in-plane susceptibility ($\chi_\perp$), a quartet-specific hybridization must be included. This is shown most clearly in Fig. 3. Here, we show best fits to the measured data using three calculation approaches, that of the traditional Bethe-ansatz, the NCA with a single hybridization that was used for $Yb_2Ir_2Ga_9$, and the NCA allowing for a different hybridization of the upper CEF quartet than that of the lower CEF quartet ($\Gamma^0_{\pm7/2,\pm5/2}\neq\Gamma^0_{\pm3/2,\pm1/2}$). Our theoretical approach also enables the calculation of γ, the low-temperature electronic contribution to specific heat. Using the best model parameters of Table I, we find 68 mJ/mol Yb K^2 and 28 mJ/mol Yb K^2 for $Yb_2Rh_3Ga_9$ and $Yb_2Ir_3Ga_9$, respectively, in reasonable agreement with measured values [45(25) mJ/mol Yb K^2 for M=Rh (Ir)]. Inelastic neutron scattering measurements of the quasielastic linewidth and x-ray absorption spectroscopy measurements of n_f are presently in progress to further validate our model.[30]

In summary, measurements of magnetic susceptibility, specific heat, and electrical resistivity have been performed on the mixed-valence compounds $Yb_2Rh_3Ga_9$ and $Yb_2Ir_3Ga_9$. Anderson impurity model calculations within the NCA approach describe the anisotropic magnetic susceptibility indicating that it is essential to include crystalline electric field effects. In $Yb_2Ir_3Ga_9$, a single hybridization of the two split CEF quartets with the conduction electrons is needed to model the anisotropic $\chi(T)$, while two different hybridizations of the two quartets are needed to fit the $\chi(T)$ data of $Yb_2Rh_3Ga_9$.

ACKNOWLEDGMENTS

One of the authors (A.A.A.) thanks J. Sereni for useful discussions. This work was sponsored by PICT 03-12742 of ANPCyT. Two of the authors (A.L., A.A.A.) are partially supported by CONICET.

*Present address: Department of Chemistry, University of Delaware, Newark, Delaware 19716, USA.
†Los Alamos National Laboratory, Los Alamos, New Mexico 87545, USA.

[1] A. C. Hewson, *The Kondo Problem to Heavy Fermions* (Cambridge University Press, Cambridge, 1993).
[2] J. C. P. Klasse, F. R. de Boer, and P. F. de Châtel, Physica B & C **106**, 178 (1981).
[3] J. L. Sarrao, C. D. Immer, Z. Fisk, C. H. Booth, E. Figueroa, J. M. Lawrence, R. Modler, A. L. Cornelius, M. F. Hundley, G. H. Kwei, J. D. Thompson, and F. Bridges, Phys. Rev. B **59**, 6855 (1999), and references therein.
[4] B. Buschinger, C. Geibel, M. Weiden, C. Dietrich, G. Cordier, G. Olesch, J. Köhler, and F. Steglich, J. Alloys Compd. **260**, 44 (1997).
[5] S. K. Dhar, C. Mitra, P. Manfrinetti, A. Palenzona, and P. Bonville, Physica B **259-261**, 150 (1999).
[6] O. Trovarelli, C. Geibel, B. Buschinger, R. Borth, S. Mederle, M. Grosche, G. Sparn, F. Steglich, O. Brosch, and L. Donnevert, Phys. Rev. B **60**, 1136 (1999).
[7] T. Okane, S.-I. Fujimori, A. Ino, A. Fujimori, S. K. Dhar, C. Mitra, P. Manfrinetti, A. Palenzona, and O. Sakai, Phys. Rev. B **65**, 125102 (2002).
[8] T. A. Costi, Phys. Rev. Lett. **80**, 1038 (1998).
[9] E. A. Goremychkin, R. Osborn, B. D. Rainford, T. A. Costi, A. P. Murani, C. A. Scott, and P. J. C. King, Phys. Rev. Lett. **89**, 147201 (2002).
[10] C. Petrovic, M. F. Hundley, R. Movshovich, P. G. Pagiluso, J. L. Sarrao, J. D. Thompson, and Z. Fisk, J. Alloys Compd. **325**, 1 (2001).
[11] C. Petrovic, M. F. Hundley, R. Movshovich, P. G. Pagiluso, J. L. Sarrao, J. D. Thompson, Z. Fisk, A. Garcia, E. Granado, I. Torriani, and C. Rettori, J. Magn. Magn. Mater. **225**, 317 (2001).
[12] S. Bobev *et al.* (unpublished).
[13] J. Niermann, B. Fehrmann, M. W. Wolff, and W. Jeitschko, J. Solid State Chem. **177**, 2600 (2004).
[14] H. Desgranges and J. W. Rasul, Phys. Rev. B **32**, R6100 (1985).
[15] A. Okiji and N. Kawakami, J. Magn. Magn. Mater. **54-57**, 327 (1986).
[16] A. Okiji and N. Kawakami, J. Magn. Magn. Mater. **76&77**, 121 (1988).
[17] V. T. Rajan, Phys. Rev. Lett. **51**, 308 (1983).
[18] P. Schlottman, Phys. Rep. **181**, 1 (1989).
[19] N. E. Bickers, D. L. Cox, and J. W. Wilkins, Phys. Rev. B **36**, 2036 (1987).
[20] A. A. Aligia, C. A. Balseiro, and C. R. Proetto, Phys. Rev. B **33**, 6476 (1986).
[21] J. Sereni (private communication).
[22] G. Zwicknagl, V. Zevin, and P. Fulde, Z. Phys. B: Condens. Matter **79**, 365 (1990).
[23] Y. N. Grin, R. E. Gladyschevskii, O. M. Sichevich, V. E. Zavodnik, Y. P. Yarmolyuk, and I. V. Rozhdestvenskaya, Kristallografiya **29**, 893 (1984) , O. M. Sichevich, V. E. Zavodnik, Y. P. Yarmolyuk, and I. V. Rozhdestvenskaya, [Sov. Phys. Crystallogr. **29**, 528 (1984)].
[24] Y. Grin and P. Rogl, Inorg. Mater. **25**, 514 (1989).
[25] V. Zevin, G. Zwicknagl, and P. Fulde, Phys. Rev. Lett. **60**, 2331 (1988).
[26] O. Gunnarsson and K. Schönhammer, Phys. Rev. B **28**, 4315 (1983).
[27] E. Müller-Hartmann, Z. Phys. B: Condens. Matter **57**, 281 (1984).
[28] E. D. Bauer, S. Bobev, J. D. Thompson, M. F. Hundley, J. L. Sarrao, A. Lobos, and A. A. Aligia, J. Phys.: Condens. Matter **16**, 4025 (2004).
[29] J. R. Taylor, *An Introduction to Error Analysis* (University Science Books, Mill Valley, California, 1982).
[30] A. D. Christianson *et al.* (unpublished).